Recent results on Light Flavor from STAR

Jie Zhao (for the STAR collaboration)

Purdue University, West Lafayette, IN, 47907, USA,
zhao656@purdue.edu

Abstract. These proceedings present an overview of the recent results on light flavor by the STAR experiment at RHIC.

Keywords: RHIC, STAR, Quark Gluon Plasma, QCD, phase diagram

1 Introduction

Relativistic heavy-ion collision is an unique tool to study the properties of the quark-gluon plasma (QGP) in quantum chromodynamics (QCD) [1]. One important goal of the heavy-ion program in RHIC-STAR is to explore the QCD phase diagram [1, 2]. At the RHIC top energy data were collected with different species from small to large collision systems, allowing studies of the high temperature QCD to extract quantitative information on the QGP. The Beam Energy Scan (BES) program with the collision energies from 7.7 to 64.2 GeV extended the studies to lower temperature and higher baryon densities on the QCD phase diagram. The main goal is to search for the turn-off of QGP signatures and signals of the first order phase transition and the critical point [2]. To further extend the coverage on the QCD phase diagram, the fixed-target mode is exploited to reach the higher baryon densities with the baryon chemical potential in the range of $\mu_B \approx$ 420-720 MeV.

Since 2010 STAR has accumulated large volume data from 200 GeV down to 7.7 GeV. A rich body of results were produced pertinent to the properties of the QCD matter. In these proceedings, we highlight selected STAR results on light flavor measurements that were presented in the "Strangeness in Quark Matter" 2019 conference. For more details the reader is referred to the STAR contributed articles in these proceedings [3–5].

2 Initial conditions

The measurement of longitudinal decorrelation of anisotropic flow can help provide a 3D image of the evolution of the QGP [6]. Using the newly installed Forward Meason Spectrometer (FMS), STAR has measured longitudinal flow decorrelations in 200 GeV Au+Au collisions (Fig. 1). Results are found to exhibit a stronger decrease with the normalized rapidity than those at the LHC [7–9]. These results provide new constraints on both the initial-state geometry fluctuations and final-state dynamics of heavy-ion collisions.

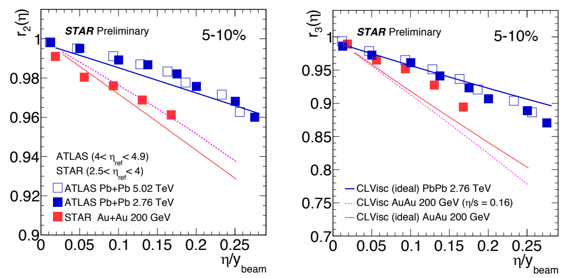

Fig. 1. De-correlation parameters r_2 (left) and r_3 (right) as a function of the normalized rapidity in 5-10% Au+Au collisions at RHIC [7] and Pb+Pb collisions at LHC [8, 9].

The measurement of the elliptic anisotropy (v_2) in small system collisions could further our understanding of the importance of the initial geometry. Figure 2 shows the v_2 obtained by difference methods in p+Au and d+Au collisions [10]. The results for different energies show a common trend with the charged particle multiplicity, which provide important insights on the nature of collectivity in small collision systems.

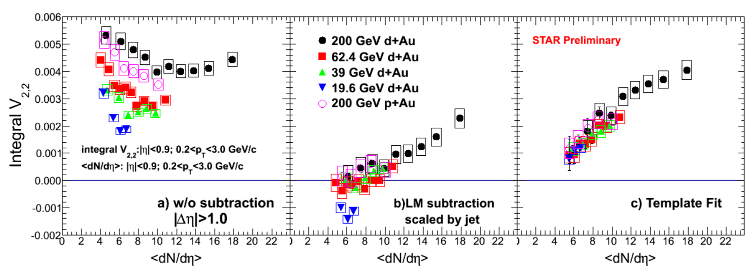

Fig. 2. Integral v_2 as function of multiplicity in p+Au and d+Au collisions [10].

3 Phase transition and critical point

The higher order fluctuation observables – higher moments of conserved quantities can be directly connected to the corresponding thermodynamic susceptibilities. It is a sensitive tool to study the criticality on the QCD phase diagram as well as to determine the freeze-out parameters [11, 12]. Figure 3 (left) shows the new measurements of the net-proton cumulants in Au+Au collisions at 54 GeV [3]. The data are compared to other energies and good agreement is found. A non-monotonic behavior as function of the collision energy is observed. Figure 3 (right) shows the 6^{th} order cumulant of the net-proton multiplicity distributions [3]. The C_6/C_2 for central Au+Au collisions at 54.4 GeV is positive while that for 200 GeV is negative, although with large uncertainties. The results are in agreement with the theoretical expectation of a smooth crossover phase transition [13, 14]. STAR also measured net-Λ cumulants, which provide insights on the flavor dependence of the freeze-out parameters [4, 15].

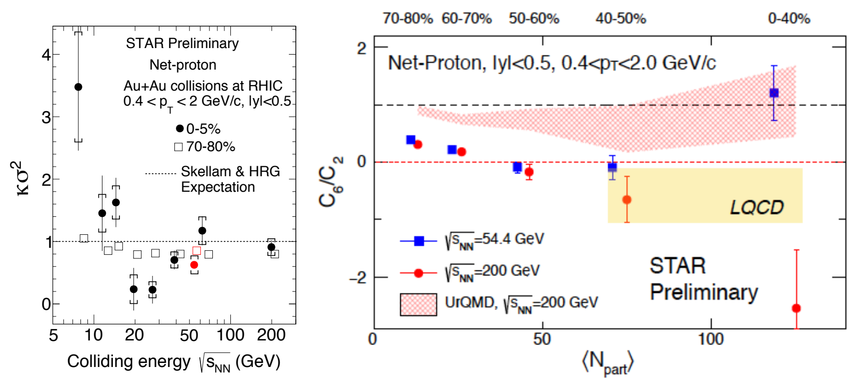

Fig. 3. Energy dependence of the net-proton moments products, $k\sigma^2$ (left), and the 6^{th} order to 2^{nd} order cumulant ratio, C_6/C_2 (right) in 54.4 and 200 GeV [3].

Production of light nuclei with small binding energies, such as the triton ($\sim$8.48 MeV) and the deuteron ($\sim$2.2 MeV), formed via final-state coalescence, are sensitive to the local nucleon density [16]. The production of these light nuclei can therefore be used to extract information of nucleon distributions at freeze-out, which could be associated with the QCD phase transition [17]. Figure 4 (left) shows that the coalescence parameter B_2 first decreases and then increase with collision energy [18]. The extracted neutron density fluctuation [19], Δn, also shows a non-monotonic behavior with collision energy (right panel of Fig. 4) [20].

One of the important QGP signatures is the nuclear modification factor R_{CP} being significantly smaller than unity at high energies. The strangeness hadron measurements from BES-I by STAR [21] show no suppression of the K_s^0 R_{cp} upto p_{T}= 3.5 GeV/c^2 . The particle type dependence of R_{CP} is found to be smaller at $\sqrt{s_{\mathrm{NN}}} \leq 11.5$ GeV (Fig. 5). These measurements point to the beam energy region below 19.6 GeV for further investigation of the deconfinement phase transition.

4 Hypertriton

The measurement of hypertriton can provide insight on hyperon-nucleon interactions [22, 23]. The HFT detector significantly improved the signal-to-background

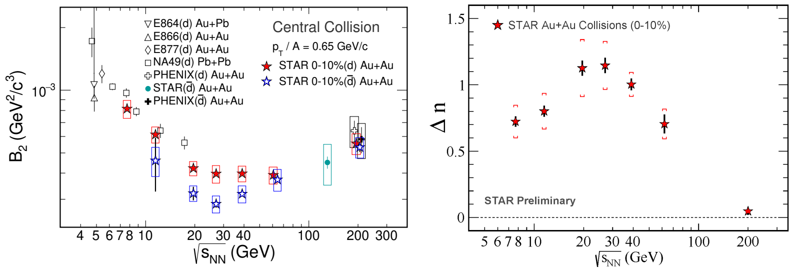

Fig. 4. Energy dependence of the coalescence parameter, B_2 (left) and the neutron density fluctuation, Δn (right) from Au+Au collisions at RHIC [18, 20].

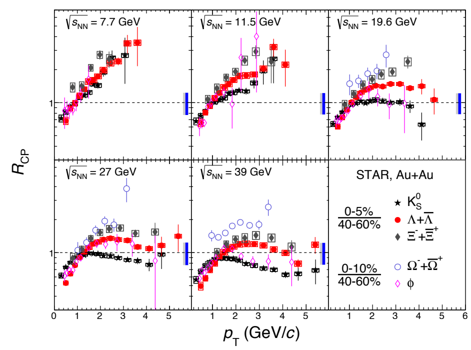

Fig. 5. R_{cp} of the $K_s^0, \Lambda, \Xi, \phi, \Omega$ in Au+Au collisions at $\sqrt{s_{\rm NN}}$ = 7.7 - 39 GeV [21].

ratio of hypertriton, thus allowing more precise determinations of the hypertriton binding energy and mass difference between hypertriton and anti-hypertriton. The STAR data [24] provide the first test of the CPT symmetry in the light hypernuclei sector. No deviation from the exact symmetry is observed.

5 Medium effect and dynamics

Lifetimes of resonances are comparable to the typical lifetime of the QGP fireball created in heavy-ion collisions. Resonances can thus be used to study the properties and evolution of the hot and dense QGP medium. K^{*0} and ϕ meson have different hadrnic cross-sections and lifetimes. Their comparisons in Fig. 6 indicate strong medium effects at RHIC and LHC [5, 25].

Di-leptons are penetrating probe to heavy-ion collisions [26]. Recent measurements show a strong enhancement in the very low $p_{\rm T}$ region. The results point to additional physics contributions, for example contributions from photon interactions in the initial magnetic field [27].

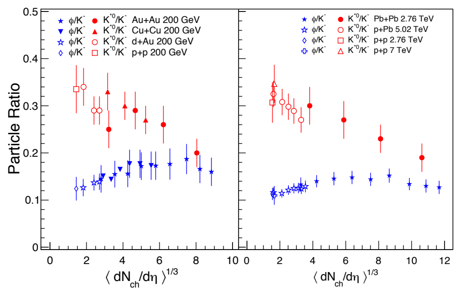

Fig. 6. K^{*0} and ϕ to K ratio as function of multiplicity from RHIC (left) [5] and LHC (right) [25].

6 Chirality, vorticity and polarization effects

Due to spin-orbit coupling, particles produced in non-central heavy-ion collisions possess large orbital angular momentum and can be globally polarized along the angular momentum direction [28]. This effect was demonstrated by the global Λ polarization measurement from STAR (left panel of Fig. 7) [29]. The data also hint a systematic splitting between Λ and $\bar{\Lambda}$, an effect expected from the initial magnetic field. Recently, STAR reported a first observation of the Λ local polarization with a quadrupole structure (right panel of Fig. 7), which could be related to the elliptic flow [30].

An electric charge separation can be induced by chirality imbalance along a strong magnetic field and is predicted to occur in relativistic heavy-ion collisions because of topological charge fluctuations and the approximate chiral symmetry restoration in QCD. This effect is called the Chiral Magnetic Effect (CME) [31]. Since the first measurement of the $\Delta\gamma$ correlator in 2009 [32], there have been extensive developments to reduce or eliminate the backgrounds [31]. Figure 8 (left) shows the results by using the invariant mass method, one of the recently developed method [33]. The extracted potential CME signal relative to the inclusive $\Delta\gamma$ in 200 GeV Au+Au collisions with two novel methods [34, 35] are summarized in right panel of Fig. 8. These data-driven estimates indicate that the possible CME signal is small, within 1-2 σ from zero [33].

7 Summary

The recent results on light flavor from the STAR experiment are overviewed. The longitudinal flow decorrelation was measured in heavy-ion data and compared to LHC data. The elliptic anisotropy is measured p+Au and d+Au collisions. These measurements will further our understanding of the importance of the initial geometry to the system evolution. The net-proton (net-Λ) cumulants, the light nuclei coalescence parameter and neutron density fluctuation are reported. All these results seem to show non-monotonic behaviors with collision energy

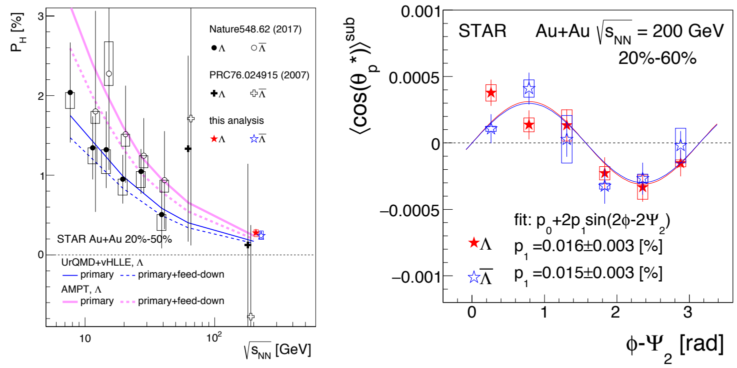

Fig. 7. (Left) Energy dependence of the global polarization of Λ and $\bar{\Lambda}$ in Au+Au collisions [29], (right) local polarization of Λ and $\bar{\Lambda}$ as a function of azimuthal angle [30].

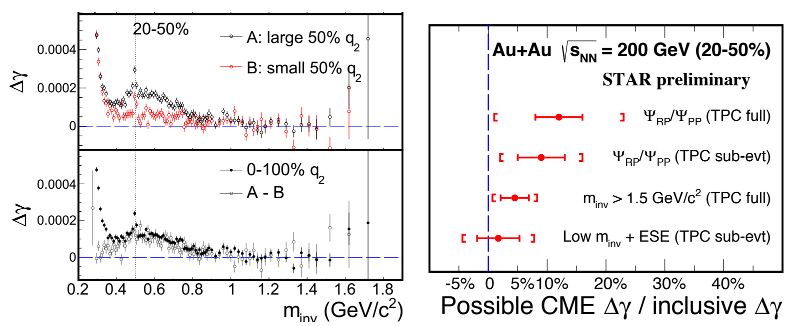

Fig. 8. (Left) $\Delta\gamma$ correlator as function of invariant [33], (right) relative contribution from possible CME signal to the measured $\Delta\gamma$ [33–35].

and may bear important implications to phase transitions and the possible critical point. The strangeness hadron production is found to be not suppressed at $\sqrt{s_{\mathrm{NN}}} \leq 11.5$ GeV, calling for further studies at low energies. The resonance ratios are measured, which indicate strong medium effects. Strong enhancement is observed in the very low p_{T} di-electron yield, which may be due to photon interactions. Hypertriton measurements are reported, which present the first test of the CPT symmetry in the light hypernuclei sector. The Λ local polarization with a quadrupole structure is observed for the first time. which needs further theoretical undertanding. Two novel data-driven methods are used to search for CME signal. The present estimates indicate that the possible CME signal is small, within 1-2 σ from zero.

Acknowledgement This work was supported by the U.S. Department of Energy (Grant No. de-sc0012910).

References

1. J. Adams et al., STAR collaboration, Nucl. Phys. A 757, 102, 2005; K. Adcox et al., PHENIX Collaboration, ibid. 757, 184 2005; B. B. Back et al., PHOBOS Collaboration, ibid. 757, 28 2005; I. Arsene et al., BRAHMS Collaboration, ibid. 757, 1 2005.
2. M. M. Aggarwal et al., STAR collaboration, arXiv:1007.2613
3. A. Pandav (for the STAR collaboration), contribution to these proceedings.
4. R. Bellwied (for the STAR collaboration), contribution to these proceedings.
5. M. Nasim (for the STAR collaboration), contribution to these proceedings.
6. P. Bozek, W. Broniowski, and J. Moreira, Phys. Rev. C 83:034911, 2011.
7. M. Nie (for the STAR collaboration), Nucl. Phys. A 982, 403, 2019.
8. V. Khachatryan et al., CMS collaboration, Phys. Rev. C 92(3):034911, 2015.
9. M. Aaboud et al., ATLAS collaboration, Eur. Phys. J. C 78(2):142, 2018.
10. S. Huang (for the STAR collaboration), Nucl. Phys. A 982, 475, 2019.
11. M. A. Stephanov, Phys. Rev. Lett. 107:052301, 2011.
12. X. Luo and N. Xu, Nucl. Sci. Tech. 28(8):112, 2017.
13. M. Cheng, etal., Phys. Rev. D 79:074505, 2009.
14. B. Friman, F. Karsch, K. Redlich, and V. Skokov, Eur. Phys. J. C 71:1694, 2011.
15. R. Bellwied, J. Hostler, P. Parotto, I. Vazquez, C. Ratti, and J. M. Stafford, Phys. Rev. C 99(3):034912, 2019.
16. L. P. Csernai and J. I. Kapusta, Phys. Rept. 131:223318, 1986.
17. H. H. Gutbrod, A. Sandoval, P. J. Johansen, A. M. Poskanzer, J. Gosset, W. G. Meyer, G. D. Westfall, and R. Stock, Phys. Rev. Lett. 37:667670, 1976.
18. J. Adam et al., STAR collaboration, Phys. Rev. C 99(6):064905, 2019.
19. K. Sun, L. Chen, C. Ko, and Z. Xu, Phys. Lett. B 774:103107, 2017.
20. D. Zhang (for the STAR collaboration), arXiv:1909.07028.
21. J. Adam et al., STAR collaboration, arXiv:1906.03732.
22. J. Chen, D. Keane, Y. Ma, A. Tang, and Z. Xu, Phys. Rept. 760:139, 2018.
23. B. I. Abelev et al., STAR collaboration, Science, 328:5862, 2010.
24. J. Adam et al., STAR collaboration, arXiv:1904.10520.
25. B. B. Abelev et al., ALICE collaboration, Phys. Rev. C 91:024609, 2015; ibid. 88:044910, 2013.
26. L. Adamczyk et al., STAR collaboration, Phys. Rev. Lett. 113(2):022301, 2014.
27. J. Adam et al., STAR collaboration, Phys. Rev. Lett. 121(13):132301, 2018.
28. Z. Liang and X. Wang, Phys. Rev. Lett. 94:102301, 2005.
29. L. Adamczyk et al., STAR collaboration, Nature, 548:6265, 2017.
30. J. Adam et al., STAR collaboration, Phys. Rev. Lett. 123, 132301, 2019.
31. J. Zhao and Fuqiang Wang, Prog. Part. Nucl. Phys. 107:200236, 2019.
32. B. I. Abelev et al., STAR collaboration, Phys. Rev. C 81:054908, 2010.
33. J. Zhao (for the STAR collaboration), Nucl. Phys. A 982, 535, 2019.
34. H. Xu, J. Zhao, X. Wang, H. Li, Z. Lin, C. Shen, F. Wang, Chin. Phys. C 42, 084103, 2018; H. Xu, X. Wang, H. Li, J. Zhao, Z. Lin, C. Shen, F. Wang, Phys. Rev. Lett. 121, 022301, 2018.
35. J. Zhao, H. Li, F. Wang, Eur. Phys. J. C 79, 168, 2019.